

Electrical Detection of Magnetization Switching in Single-Molecule Magnets

Amjad Alqahtani^{1 §}, DaVonne Henry,^{1 §} Lubomír Havlíček,² Luke St. Marie¹, Jakub Hrubý^{2a}, Antonín Sojka^{2b}, Morgan Hale³, Samuel Felsenfeld⁴, Abdelouahad El Fatimy⁵, Rachael L. Myers-Ward⁶, D. Kurt Gaskill⁷, Ivan Nemeč^{2,8}, Petr Neugebauer², Amy Y. Liu^{1*} and Paola Barbara^{1*}.*

¹ Department of Physics, Georgetown University, Washington, DC 20057, USA.

² Central European Institute of Technology, CEITEC BUT, Purkyňova 656/123, 61200 Brno, Czech Republic.

³ Department of Math, Computer Science, and Physics, Roanoke College, Roanoke, VA 24153, USA.

⁴ Department of Physics, University of Maryland, College Park, MD 20742, USA.

⁵ Institute of Applied Physics, Mohammed VI Polytechnic University, Lot 660, Hay Moulay Rachid Ben Guerir, 43150, Morocco.

⁶ U.S. Naval Research Laboratory, Washington, DC 20375, USA.

⁷ Institute for Research in Electronics and Applied Physics, University of Maryland, College Park, MD 20742, USA.

⁸ Department of Inorganic Chemistry, Faculty of Science, Palacký University Olomouc, Olomouc, 77146 Czech Republic.

Currently at:

^a National High Magnetic Field Laboratory, 1800 E. Paul Dirac Drive Tallahassee, FL 32310, USA

^b Department of Physics, University of California, Santa Barbara, CA 93106, USA.

[§]These authors contributed equally to this work.

* e-mail: ivan.nemec@upol.cz, Amy.Liu@georgetown.edu, Paola.Barbara@georgetown.edu

Single-molecule magnets (SMMs) with chemically tailorable properties are potential building blocks for quantum computing, high-density magnetic memory, and spintronics.^{1 2 3,4} These applications require isolated or few molecules on substrates, but studies of SMMs have mainly focused on bulk crystals. Moreover, fabrication of SMM-based devices and electrical detection of the SMM magnetic state are still coveted milestones that have so far been achieved mainly for double-decker rare-earth phthalocyanines at temperatures below 1 K.⁵⁻⁸ Here we demonstrate electrical detection of magnetization switching for a modification of the archetypal SMM Mn₁₂, up to 70 K, based on the supramolecular spin valve effect⁵ with graphene quantum dots⁹. Notably, the exchange interaction between the molecules and the graphene, as well as the dot-mediated intermolecular interaction, can be directly extracted from the electrical response, opening the way to an effective characterization of the quantum properties of different types of SMMs in a wide temperature range.

Single-molecule magnets (SMMs) consist of a core of magnetic ions embedded in a ligand shell. They are the smallest units of matter exhibiting magnetic remanence beyond isolated atoms^{10,11}, with the advantage that they can be chemically controlled by changing the ligand shell. Their large spin and strong magnetic anisotropy create an energy barrier to magnetization reversal and give rise to magnetic bistability, leading to relaxation times that can be as long as years at low temperatures¹². An SMM-based magnetic memory device would have areal density a thousand times the current state of the art of about 1 Tbit/in².¹³ Moreover, SMMs show quantized behavior and can be described by a single-spin Hamiltonian, opening the possibility to create a large number of identical qubits with a bottom-up approach.

The integration of SMMs in nanoelectronic devices requires controlled placement of the molecules on device surfaces. There are successful deposition methods that do not alter their magnetic properties^{14,15,16}, and a few reports demonstrated an electrical readout of the SMM magnetic state by dropcasting a dilute solution of SMMs. While the dropcast method does not afford controlled placement of molecules on the device, it was used to successfully fabricate two types of devices: molecular junctions and supramolecular spin valves.^{5-8,17-21} In molecular junctions, SMMs bridge electrical contacts, the electrical current flows through the molecule, and the current depends on the SMM magnetic state. For supramolecular spin valves, the magnetic alignment of the SMMs on the surface of carbon-nanotube or graphene quantum dots changes the electrical current through the dots. Both effects were measurable below 2 K and represented pioneering studies of the electrical read-out of SMM magnetic moments.

In this work, we expand these experiments to a modification of Mn₁₂ deposited on quantum dots of graphene epitaxially grown on SiC (Figure 1a). We show that the SMMs affect the current through the graphene quantum dots (GQDs) in a temperature range from a few kelvins to about

70 K. The switching of the molecules' magnetization causes jumps between GQD conductance states, from which we extract the exchange interaction between the SMMs and the GQDs. Similarly to previous works, we cannot control the position of the molecules on the graphene surface, so the exchange interaction varies with an average value around 0.1 meV. Even with SMM powder-coated samples, the supramolecular spin valve effect is caused by only a few molecules closest to the GQD surface since the exchange interaction is very short-ranged. Temporal studies of the conductance jumps also unveil the occurrence of an antiferromagnetic intermolecular interaction that is mediated by the GQD. We determine experimentally that the strength of this intermolecular interaction is higher than 0.5 meV and lower than 1.4 meV for our system.

The first SMM, $\text{Mn}_{12}\text{-ac}$, $[\text{Mn}_{12}\text{O}_{12}(\text{O}_2\text{CR})_{16}(\text{H}_2\text{O})_4] \cdot 4\text{H}_2\text{O} \cdot 2\text{CH}_3\text{CO}_2\text{H}$, where $\text{R} = \text{CH}_3$, has a magnetic core of 12 Mn ions that gives rise to a total spin $S = 10$.^{22 23} The ligand field breaks the degeneracy of the $2S + 1$ spin states such that in zero magnetic field, the energies are Dm_s^2 , where D is the easy-axis magnetic anisotropy parameter. The lowest energy states, $m_s = \pm 10$, are separated by an energy barrier $\Delta \sim |D|S^2$, where $\Delta/k_B \approx 70$ K. For this work, we use a modified version of Mn_{12} synthesized with chlorinated ligands, $\text{R} = \text{CHCl}_2$, as shown in Figure 1b, to promote interaction of the molecules with the graphene surface via charge transfer²⁴. The phase purity of all the batches of $\text{Mn}_{12}\text{-CHCl}_2$ used in this study was confirmed by XRPD [see Methods and Supplementary Information (SI)]. The magnetic properties of a $\text{Mn}_{12}\text{-CHCl}_2$ powder sample are shown in Figure 1c. As expected for Mn_{12} , the molecules exhibit clear hysteresis with a blocking temperature around 3 K along with steps indicating resonant quantum tunneling of the magnetization.²⁵

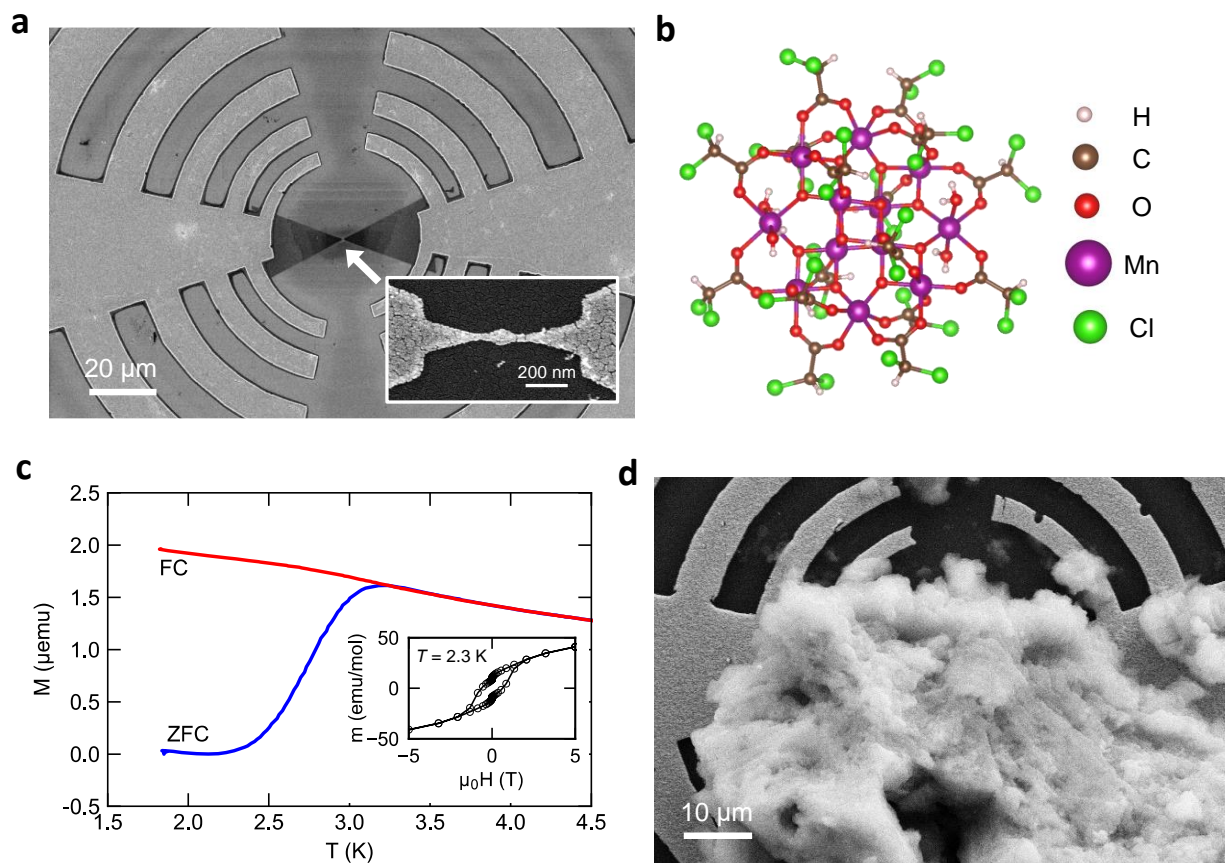


Figure 1: Graphene quantum dots coated with $\text{Mn}_{12}\text{-CHCl}_2$ powder. **a**, SEM image of completed device showing graphene “bowtie” structure in the center and gold, log-periodic toothed antennas that make up part of the contacts for other applications.²⁶ Inset: Detail of quantum dot shown mid-fabrication with gold protection layer. Arrays of these devices are typically fabricated on each graphene-on-SiC chip. **b**, Structure of $\text{Mn}_{12}\text{-CHCl}_2$. **c**, Magnetization vs. temperature measurements for $\text{Mn}_{12}\text{-CHCl}_2$ showing results for cooling in magnetic field (red) and for increasing temperature after cooling in zero magnetic field (blue). The red and blue curves meet at the blocking temperature, which is about 3 K for this molecule. Inset: Hysteresis loop for $\text{Mn}_{12}\text{-CHCl}_2$. **d**, SEM image of device A3 after depositing powder SMM sample.

Arrays of GQDs with the same geometry were fabricated by nanopatterning epitaxial graphene grown on SiC, as described in our previous work and in the Methods.⁹ The devices have a bowtie structure, with a 60-80 nm dot between the graphene source and drain leads, which are connected to the dot by nanoconstrictions, as seen in Figure 1a. The dot introduces a quantum confinement gap, resulting in thermally activated behavior of the source-drain current in a wide temperature

range. We use conductance vs. temperature measurements to determine the activation energy.^{9,26-}

²⁸ For devices used in this work, the activation energy can be determined to within 0.05 meV based on analysis of the Arrhenius plots shown in the SI.

Dry Mn₁₂-CHCl₂ powder was deposited on GQD devices in ambient conditions to avoid residues from solvents (see Figure 1d.) After depositing the Mn₁₂-CHCl₂ molecules, we observed discrete jumps in the conductance, as well as a change in the activation energy, as shown in Figure 2a. This behavior was observed in more than seven devices on two different graphene chips but was systematically measured in the four devices presented in this work (see SI for a summary of the devices).

The change in activation energy is likely due to doping by SMMs on the graphene electrodes, as our deposition leaves SMM powder not just on the quantum dot, but also on the triangular graphene electrodes around the dot. On graphene field-effect transistors, we find that Mn₁₂-CHCl₂ hole-dopes the graphene, as has been reported previously.²⁴ The discrete jumps in conductance, however, only appear in the SMM-coated GQD devices, indicating that they arise from the presence of SMMs on the dot itself.

To investigate the behavior of switching between conductance states, the conductance through the coated dot was measured over time by applying a constant bias voltage V_{SD} as the devices were cooled first in zero magnetic field, and then in a field of 3 T, above the Mn₁₂ saturation field B_{sat} , as shown in Figure 2b. In zero magnetic field, above the blocking temperature T_B , the conductance switches between a lower state and a short-lived upper state. The switching occurs less frequently as the device is cooled below the SMM T_B until ultimately the conductance settles in the lower state below 2 K. With a 3 T magnetic field, the switching disappears, and the conductance remains in the upper state as the device is cooled.

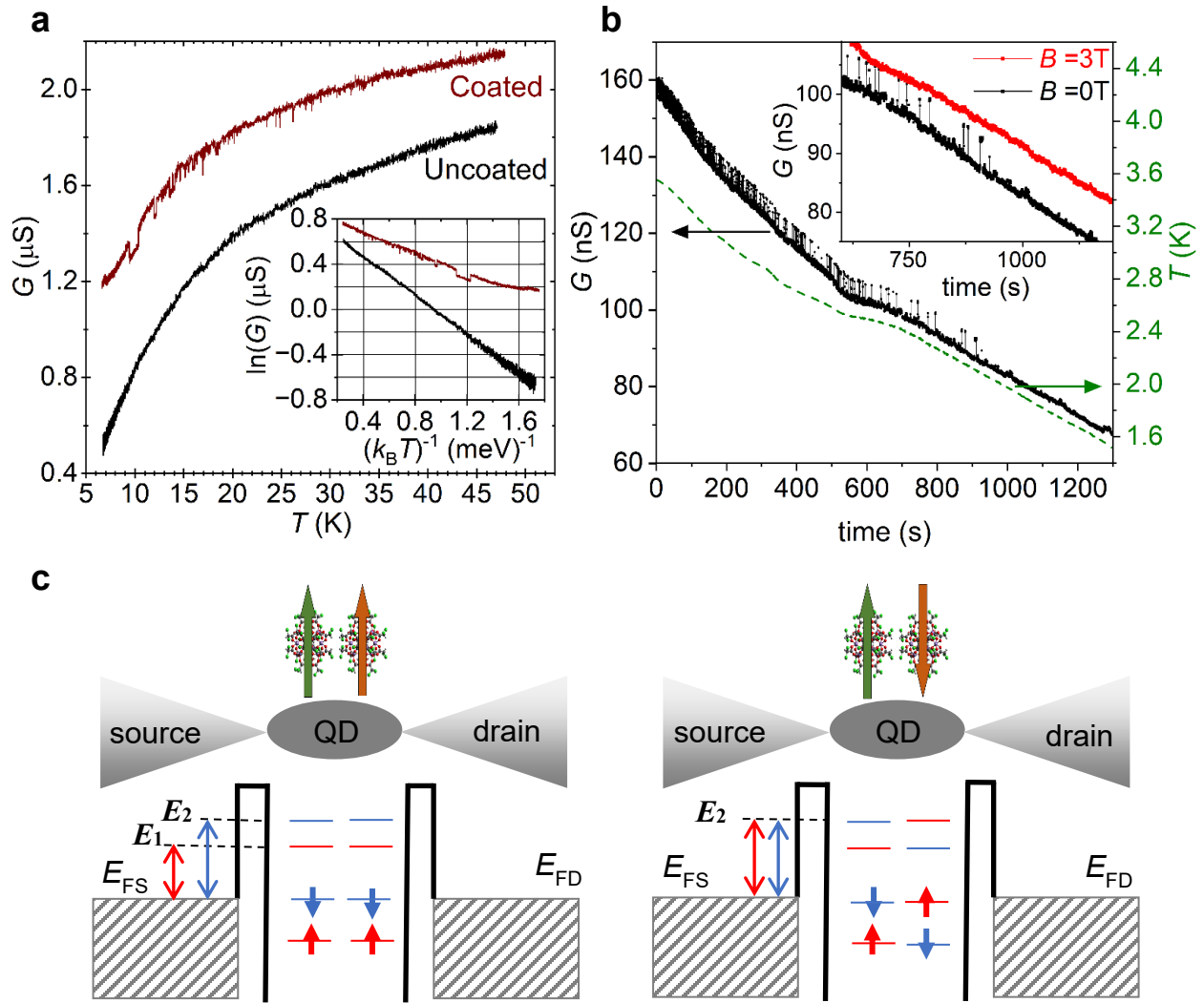


Figure 2. **Electronic transport in Mn₁₂-coated GQDs.** **a**, Conductance vs. temperature measured at a constant source-drain bias voltage $V_{\text{SD}} \leq 5$ mV for device A3, before and after depositing the Mn₁₂-CHCl₂ SMMs. Discrete jumps are observed due to the magnetization switching of the molecules. Inset: Arrhenius plot of the conductance shows that the activation energy changes after depositing the molecules. **b**, Conductance vs. time at $V_{\text{SD}} = 450$ mV, as device A7 is cooled to 1.5 K at $B = 0$ T (black). Inset: Zoomed-in image of the $B = 0$ T data (black) along with the corresponding field-cooled measurement at $B = 3$ T (red), where no switching occurs and the conductance is in the upper state. **c**, Illustration of how the magnetic alignment of two SMMs influences the electronic energy levels in the GQD. The Fermi-level of the source and drain are denoted by E_{FS} and E_{FD} respectively.

The presence of two conductance states and their magnetic-field dependence are suggestive of the supramolecular spin-valve effect first reported for Tb SMMs on carbon nanotube quantum dots.⁵ In that work, below the SMM blocking temperature, the authors measured hysteretic switching between two carbon nanotube conductance states as a function of magnetic field.⁵ We measure similar hysteretic behavior also for the conductance of our coated graphene quantum dots, as shown in Figure S7 in the Supplementary Information. This hysteresis is angle dependent, where the field oriented nearly parallel to the device substrate maximizes the presence of the two conductance states. All the magnetic field measurements presented in this work were performed with this orientation. We attribute this angle dependence to the magnetic anisotropy of Mn₁₂. In contrast to previous investigations of the supramolecular spin-valve effect, where the two conductance states could be only be measured by using a gate electrode to tune away from the Coulomb blockade regime,⁵ we use ungated devices. Our quantum dots are patterned from graphene on SiC, which precludes the bottom gate configuration. Although top gates could be fabricated, they would prevent the direct deposition of molecules on the graphene. Nevertheless, the effects of the SMMs on the electronic transport in the ungated quantum dots can clearly be measured.

We consider a simple model of two SMMs on the GQD as shown in Figure 2c. The interaction between the molecules and the graphene locally spin-splits the discretized states in the dot, thereby dividing the original dot into coupled dots. The device current is determined by the activation energy required for an electron to tunnel through the coupled dots. The GQD conductance can be expressed as the sum of the contribution of both spin channels. In the case where the molecules are ferromagnetically aligned, $G_{\text{FM}} = G_0(e^{-E_1/k_B T} + e^{-E_2/k_B T})$, where E_1 and E_2 are the

activation energies shown in Figure 2c. In the case in which the molecules are antiferromagnetically aligned, $G_{AFM} = 2G_0 e^{-E_2/k_B T}$. From these expressions, we extract:

$$\Delta E = E_2 - E_1 = k_B T \ln\left(2 \frac{G_{FM}}{G_{AFM}} - 1\right) . \quad 1$$

This simple model provides a qualitative explanation of Figure 2b. In zero magnetic field, above T_B , the molecules can switch their magnetization either by quantum tunneling or by thermally-assisted tunneling, consistent with the occurrence of conductance jumps. Also, their switching frequency decreases as the temperature approaches T_B . Below T_B , the switching stops, and conductance jumps disappear. When the devices are field-cooled above B_{sat} , the molecules are always aligned, as evidenced by the device cooling in the higher conductance state.

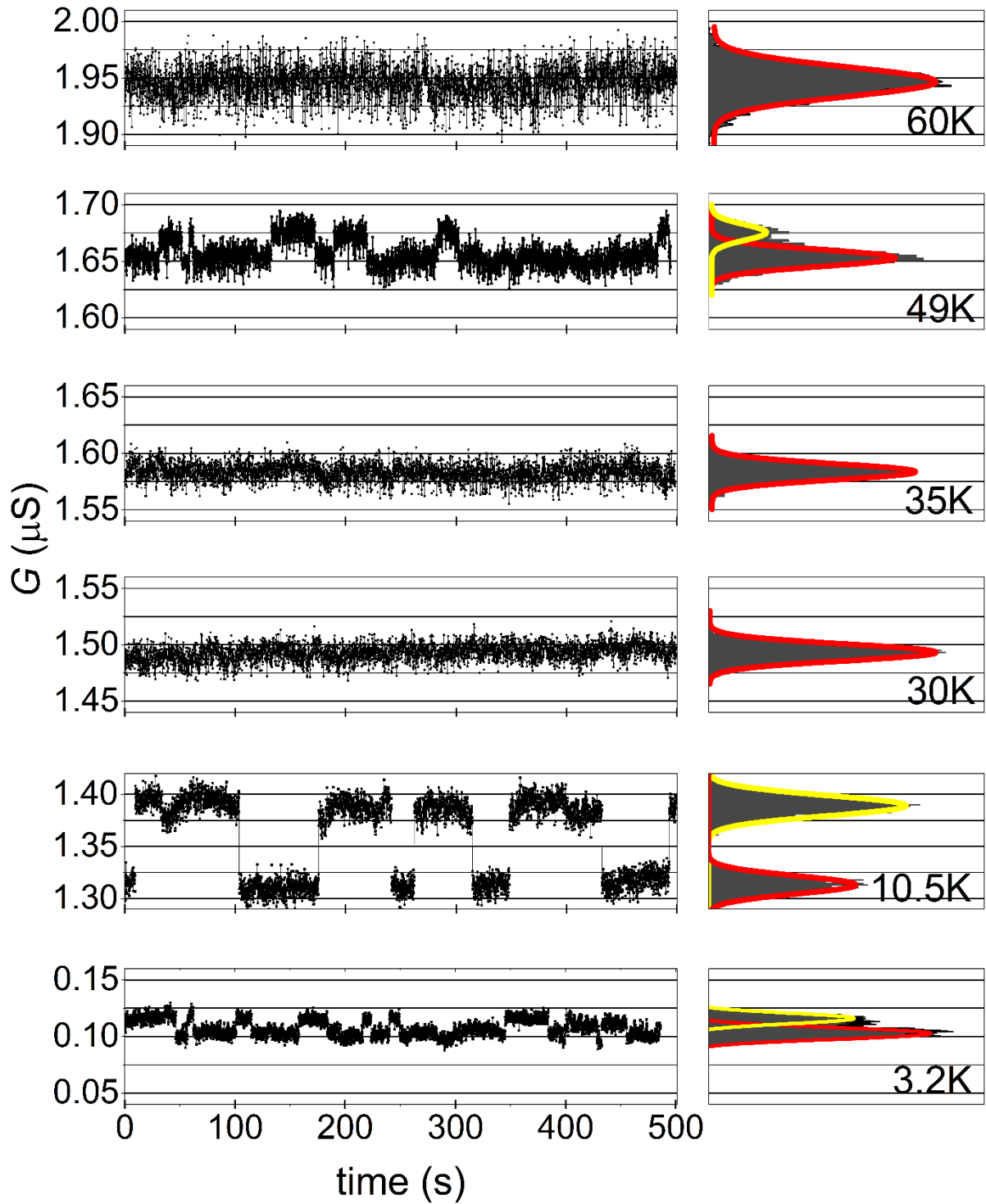


Figure 3: **Conductance vs. time measurements.** Measurements were taken on device A3 at a constant bias voltage $V_{SD} \leq 5\text{mV}$ at 6 different temperatures. Histograms were created for each time series and fit to Gaussians (yellow and red curves) to aid in the identification of the discrete conductance states. The current preamplifier sensitivity was set to 10^{-9} A/V for all temperatures

except 3.2 K where the sensitivity was set to 10^{-10} A/V to account for the smaller current at low temperatures.

To test this interpretation quantitatively, we measured conductance vs. time at different temperatures for different devices at a small fixed bias voltage ($V_{SD} \leq 5$ mV) to avoid Joule heating and hot-electron effects.⁹ In Figure 3, clear conductance jumps can be distinguished at 3.2 K and 10.5 K. Notably, the jumps disappear between 30 K and 40 K but reappear at about 50 K. This could be related to transitions to spin manifolds differing from the $S = 10$ ground state. For example, signatures attributed to the $S = 10$ to $S = 9$ transition have been observed around 40 K.^{29,30} At 60 K, the increased width of the conductance histogram indicates fast switching between states that cannot be distinguished for this device. Using Equation 1, we calculate ΔE for each temperature with clear jumps. The same measurements were performed on other devices and yielded similar temperature-independent values of $\Delta E \approx 0.1$ meV (see Figure 4a.) This supports our model where ΔE arises from a temperature-independent interaction between the graphene and the SMMs. Note that Equation 1 only applies in the temperature range with thermally-activated conductance. See SI for error analysis and data for other devices.

A possible origin of ΔE is Zeeman splitting of the spin states in the GQD from the SMM dipolar magnetic field. An estimate of the dipolar field is about 0.05 T for a Mn_{12} molecule centered 9 Å above the graphene. If the $\Delta E \approx 0.1$ meV were due to the Zeeman effect, it would imply a field of about 1 T at the graphene surface, requiring around 20 neighboring molecules with aligned moments near the surface, conceivably within a single crystallite. However, long-range magnetic ordering within the crystallite is unlikely under the conditions of our experiments.¹² A more likely explanation is a graphene-SMM exchange interaction that can be much stronger than the SMM-induced Zeeman effect. An individual molecule near the surface can produce the measured splittings, as discussed below. Moreover, the exchange interaction is very short-ranged and likely

limited to a few molecules that are closest to the GQD. Even though our devices are coated with powder, the short-ranged exchange interaction supports the use of a few-molecule model to explain the conductance switching.

To estimate the proximity-induced exchange splitting of graphene electronic states, we performed density functional theory calculations of a $\text{Mn}_{12}\text{-CHCl}_2$ molecule on graphene, with two different orientations of the molecular easy axis: parallel and perpendicular to the graphene. The distance between the graphene and the closest atom on the molecule was set to 3.25 \AA , which is in the range of energetically favorable separations for various orientations in our calculations. We focused on the eight degenerate states at the Dirac point in intrinsic graphene. The interaction with the molecule breaks the symmetry and splits the states as shown in Figure 4b for the perpendicular orientation. The splitting of up to 0.10 meV for the four spin-degenerate levels is caused by the exchange interaction. This is consistent with values estimated from our experiments as seen in Figure 4a, as well as estimates from transport measurements of bottom-gated SMM-coated quantum dots³¹ and related theoretical work.³² While the combined structure shows spin-up magnetization, the proximity-induced exchange interaction shifts the graphene spin-up states at the Dirac point higher in energy, suggesting an antiferromagnetic interaction between the molecule and graphene. Results for the parallel case are included in the SI.

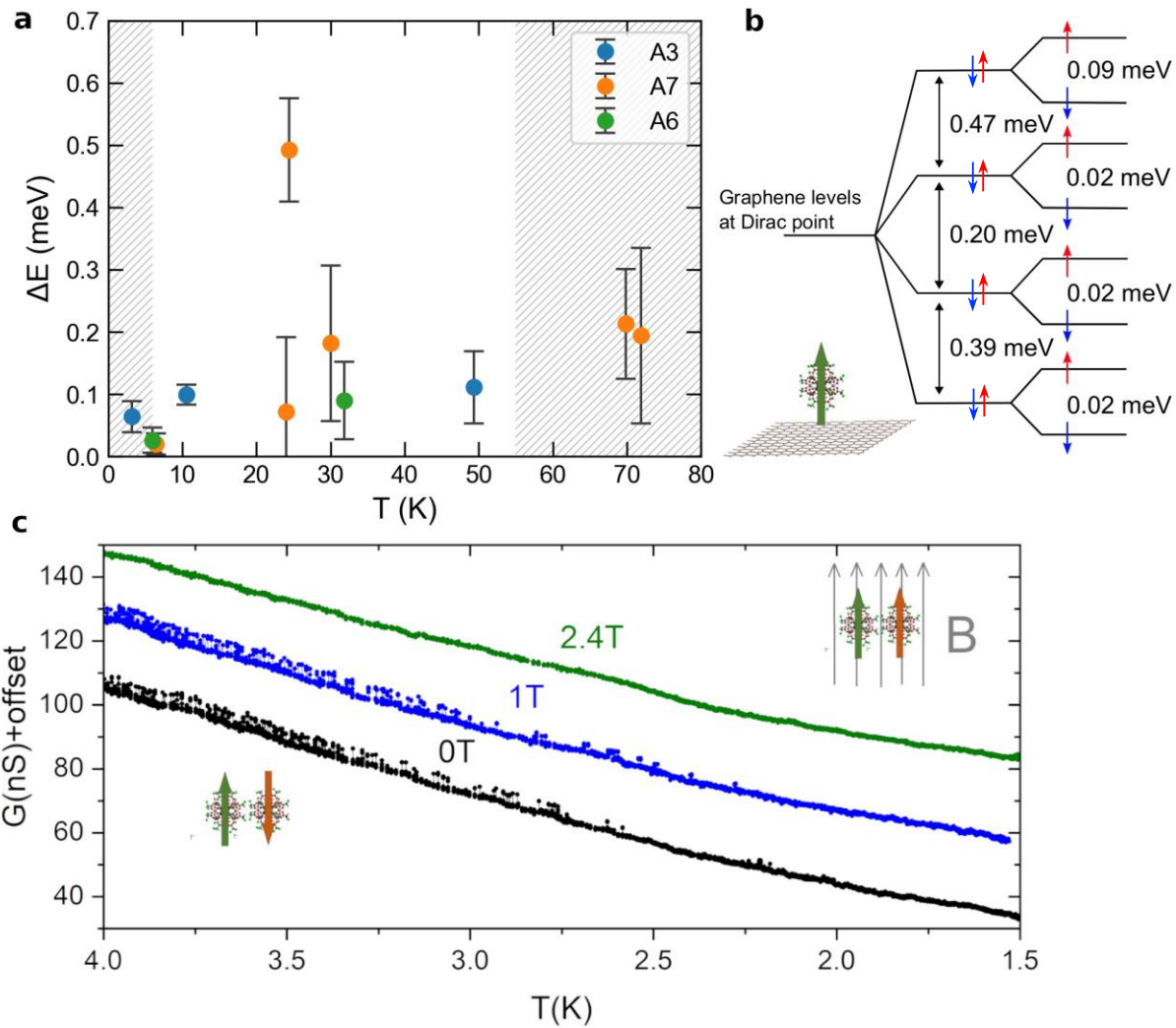


Figure 4: **Interaction energies.** **a**, Experimentally determined exchange energies for three devices. The hatched areas indicate temperature regions outside of thermal activation behavior. **b**, Energy level diagram determined from DFT of a $\text{Mn}_{12}\text{-CHCl}_2$ molecule on graphene, with the molecular easy axis perpendicular to the graphene surface. The degenerate levels from the Dirac point in graphene are split by non-magnetic interactions with the molecule, and further split by the exchange interaction. **c**, Conductance vs. temperature of device A7 measured at different magnetic fields. The threshold field above which conductance jumps are suppressed is between 1 T and 2.4 T.

We also note that in zero magnetic field, at low temperature, the lower conductance state is clearly preferred by the coated GQDs, as shown in Figure 2b. This suggests that the molecules are antiferromagnetically coupled, seemingly contradicting the idea that even in crystals, the molecules do not order magnetically. However, a quantum-dot-mediated spin-spin interaction

between SMMs has been proposed by Krainov et al,⁸ who predicted a gate-tunable interaction between SMMs that arises from charging effects when the molecules divide a single carbon nanotube quantum dot into multiple coupled dots.

To probe this quantum-dot-mediated intermolecular interaction ΔE_{IM} for our SMM-coated GQDs, we performed measurements similar to those shown in Figure 2b by cooling the device in different applied magnetic fields. The results are in Figure 4c. We find that the conductance jumps are still present for an applied field of 1 T, while for 2.4 T, the Zeeman interaction between the Mn₁₂ and the external field prevails over the antiferromagnetic intermolecular interaction and the jumps disappear. Therefore, we can extract an upper and lower bound for the strength of this antiferromagnetic interaction, namely $0.5 \text{ meV} < \Delta E_{\text{IM}} < 1.4 \text{ meV}$. These values are consistent with previous work.⁸

A remaining puzzle is the slow rate of magnetization switching of the SMMs compared to previous measurements on Mn₁₂-acetate crystals and aligned powders.^{25,33} It is possible that the antiferromagnetic intermolecular interaction mediated by the graphene substrate in our system affects the SMM relaxation rate,³⁴ which is an interesting avenue for future investigation.

Remarkably, from direct measurements of two electrical current values in our SMM-coated GQD devices, we can determine the quantum-dot-mediated intermolecular interaction and the SMM-graphene exchange interactions, without the need of a gate electrode and without introducing any fitting parameters. Moreover, the occurrence of the current switching in a wide temperature range may allow the investigation of excited spin manifolds that are not accessible at low temperature.^{29,30} These experiments open the way to studies of other types of SMMs, while providing a platform for the electrical readout of their magnetic switching.

Acknowledgments

This work at Georgetown University was supported by the U.S. Office of Naval Research (N00014-16-1-2674 and DURIP N00014-17-1-2436) and the U.S. National Science Foundation (ECCS-1610953 and DMR-1950502). The work at CEITEC was supported by GACR EXPRO, GACR Laguta, and LTAUSA 19060. I.N. acknowledges the financial support from institutional sources of the Department of Inorganic Chemistry, Palacký University Olomouc, Czech Republic. Research performed at the Naval Research Laboratory was supported by the Office of Naval Research. The authors thank Mark Pederson, Gen Yin, and Jorge Navarro Giraldo for helpful discussions and Linli Meng and Yanfei Yang for the Graphene Waves material characterization.

Author Contributions

Device fabrication and transport measurements were performed by A.A., D.H. and L.SM. I.N. and L.H. synthesized and characterized the SMMs. R.L.M.-W. and D.K.G. synthesized and characterized the NRL graphene on SiC. D.H. and M.H. performed the DFT calculations. P.B., P.N., A.Y.L., I.N. designed the project. All authors contributed to the data analysis, the discussion of the results and the manuscript preparation.

Competing Interests

The authors declare no competing financial interests.

Methods

Compound Preparation

All chemicals and solvents were used as received. All preparations and manipulations were performed under aerobic conditions. $[\text{Mn}_{12}\text{O}_{12}(\text{O}_2\text{CMe})_{16}(\text{H}_2\text{O})_4]$ (**1**) was prepared as previously described.³⁵ The compound $[\text{Mn}_{12}\text{O}_{12}(\text{O}_2\text{CHCl}_2)_{16}(\text{H}_2\text{O})_4]$ (**2**) was prepared by modified reported synthesis.³⁶ This modified approach yielded good quality crystals in shorter time. A solution of compound **1** (1 mmol) in CH_2Cl_2 (50 ml) was treated by excess of dichloroacetic acid (40 mmol). The solution was stirred overnight, and the solvent was filtered through paper filter. The solution was left to crystalize undisturbed in dark at room temperature. After a week the solvent was removed in vacuo yielding (40 %) dark brown crystals of **2**.

Device Fabrication

Epitaxial graphene grown by Si sublimation from SiC substrates was obtained from Naval Research Laboratory³⁷ and Graphene Waves. The graphene was patterned into arrays of quantum dots using electron-beam lithography to fabricate multiple devices on one chip. Cr/Au electrical contacts were deposited using magnetron sputtering. Details of this QD fabrication process were reported in previous work.^{9,26-28}

The QDs were coated with SMMs using a dry deposition method in order to avoid the presence of solvent residues that may be left on the graphene surface when depositing the molecules by dropcast of dilute solutions. Small aggregates of $\text{Mn}_{12}\text{-CHCl}_2$ powder were placed on the sample using sharp tweezers. The aggregates were positioned on the devices using the probes of micromanipulators under an optical microscope. The device coating was then checked by imaging the region of the graphene bowties using a SEM (see supplementary information)

Density Functional Theory Calculations

The interaction between graphene and an adsorbed molecule of $\text{Mn}_{12}\text{-CHCl}_2$ was calculated via Density Functional Theory using the Vienna *ab initio* Simulation Package (VASP).^{38,39} Spin-polarized ground-state calculations were performed using the projector-augmented wave (PAW) method.^{40,41} Perdew-Burke-Ernzerhof (PBE) functionals were used to account for the exchange-correlation energy and van der Waals interactions are included using the optimized exchange functional optB86b.^{42,43} A 12x12 graphene supercell was used to simulate an isolated molecule on a graphene surface. The K and K' points of the graphene Brillouin zone fold onto the Γ point for the supercell. A 2x2x1 Γ -centered k-point sampling was used for calculating the energy. A gaussian smearing parameter of 0.05 eV was used. The plane-wave cutoff was 500 eV, and the self-consistency threshold was set to 10^{-5} eV. Structural relaxations were performed until the magnitude of all forces was less than 0.1 eV/Å.

To investigate the SMM-induced exchange splitting of electronic states in graphene, we compared spin-polarized and non-spin-polarized band energies, focusing on states derived from the Dirac point in graphene. Non-spin-polarized states were matched with their spin-polarized counterparts based on their site- and orbital-projected character. The difference in energy between a spin-up and spin-down state associated with the same non-spin-polarized state was identified as the exchange splitting.

- 1 Guo , F.-S. & M. Day, B. C., Yan-Cong Tong , Ming-Liang Mansikkamäki , Akseli Layfield , Richard A. Magnetic hysteresis up to 80 kelvin in a dysprosium metallocene single-molecule magnet. *Science* (2018). <https://doi.org/DOI: 10.1126/science.aav0652>
- 2 Bayliss, S. L. *et al.* Optically addressable molecular spins for quantum information processing. *Science* **370**, 1309+ (2020). <https://doi.org/10.1126/science.abb9352>
- 3 Zadrozny, J. M., Niklas, J., Poluektov, O. G. & Freedman, D. E. Millisecond Coherence Time in a Tunable Molecular Electronic Spin Qubit. *Acs Central Science* **1**, 488-492 (2015). <https://doi.org/10.1021/acscentsci.5b00338>
- 4 Bogani, L. & Wernsdorfer, W. Molecular spintronics using single-molecule magnets. *Nature Materials* **7**, 179-186 (2008). <https://doi.org/10.1038/nmat2133>
- 5 Urdampilleta, M., Klyatskaya, S., Cleuziou, J. P., Ruben, M. & Wernsdorfer, W. Supramolecular spin valves. *Nature Materials* **10**, 502-506 (2011). <https://doi.org/10.1038/nmat3050>
- 6 Candini, A., Klyatskaya, S., Ruben, M., Wernsdorfer, W. & Affronte, M. Graphene Spintronic Devices with Molecular Nanomagnets. *Nano Letters* **11**, 2634-2639 (2011). <https://doi.org/10.1021/nl2006142>
- 7 Vincent, R., Klyatskaya, S., Ruben, M., Wernsdorfer, W. & Balestro, F. Electronic read-out of a single nuclear spin using a molecular spin transistor. *Nature* **488**, 357-360 (2012). <https://doi.org/10.1038/nature11341>
- 8 Krainov, I. V. *et al.* Giant Magnetoresistance in Carbon Nanotubes with Single-Molecule Magnets TbPc2. *Acs Nano* **11**, 6868-6880 (2017). <https://doi.org/10.1021/acsnano.7b02014>
- 9 El Fatimy, A. *et al.* Epitaxial graphene quantum dots for high-performance terahertz bolometers. *Nature Nanotechnology* **11**, 335+ (2016). <https://doi.org/10.1038/nnano.2015.303>
- 10 Donati, F. *et al.* Magnetic remanence in single atoms. *Science* **352**, 318-321 (2016). <https://doi.org/10.1126/science.aad9898>
- 11 Natterer, F. D. *et al.* Reading and writing single-atom magnets. *Nature* **543**, 226+ (2017). <https://doi.org/10.1038/nature21371>
- 12 Christou, G., Gatteschi, D., Hendrickson, D. N. & Sessoli, R. Single-molecule magnets. *Mrs Bulletin* **25**, 66-71 (2000). <https://doi.org/10.1557/mrs2000.226>
- 13 Fontana, R. E. & Decad, G. M. Moore's law realities for recording systems and memory storage components: HDD, tape, NAND, and optical. *Aip Advances* **8** (2018). <https://doi.org/10.1063/1.5007621>
- 14 Gabarro-Riera, G., Aromi, G. & Sanudo, E. C. Magnetic molecules on surfaces: SMMs and beyond. *Coordination Chemistry Reviews* **475** (2023). <https://doi.org/10.1016/j.ccr.2022.214858>
- 15 Erler, P. *et al.* Highly Ordered Surface Self-Assembly of Fe-4 Single Molecule Magnets. *Nano Letters* **15**, 4546-4552 (2015). <https://doi.org/10.1021/acs.nanolett.5b01120>
- 16 Gagnaniello, L. *et al.* Uniaxial 2D Superlattice of Fe-4 Molecular Magnets on Graphene. *Nano Letters* **17**, 7177-7182 (2017). <https://doi.org/10.1021/acs.nanolett.6b05105>
- 17 Heersche, H. B. *et al.* Electron transport through single Mn-12 molecular magnets. *Physical Review Letters* **96** (2006). <https://doi.org/10.1103/PhysRevLett.96.206801>
- 18 Jo, M. H. *et al.* Signatures of molecular magnetism in single-molecule transport spectroscopy. *Nano Letters* **6**, 2014-2020 (2006). <https://doi.org/10.1021/nl061212i>
- 19 Zyazin, A. S., van der Zant, H. S. J., Wegewijs, M. R. & Cornia, A. High-spin and magnetic anisotropy signatures in three-terminal transport through a single molecule. *Synthetic Metals* **161**, 591-597 (2011). <https://doi.org/10.1016/j.synthmet.2010.11.050>
- 20 Misiorny, M. *et al.* Probing transverse magnetic anisotropy by electronic transport through a single-molecule magnet. *Physical Review B* **91** (2015). <https://doi.org/10.1103/PhysRevB.91.035442>

- 21 Pei, T. *et al.* Exchange-induced spin polarization in a single magnetic molecule junction. *Nature Communications* **13** (2022). <https://doi.org/10.1038/s41467-022-31909-w>
- 22 Lis, T. PREPARATION, STRUCTURE, AND MAGNETIC-PROPERTIES OF A DODECANUCLEAR MIXED-VALENCE MANGANESE CARBOXYLATE. *Acta Crystallographica Section B-Structural Science* **36**, 2042-2046 (1980). <https://doi.org/10.1107/s0567740880007893>
- 23 Sessoli, R., Gatteschi, D., Caneschi, A. & Novak, M. A. MAGNETIC BISTABILITY IN A METAL-ION CLUSTER. *Nature* **365**, 141-143 (1993). <https://doi.org/10.1038/365141a0>
- 24 Zhu, X. C., Hale, A., Christou, G. & Hebard, A. F. Electronegative ligands enhance charge transfer to Mn-12 single-molecule magnets deposited on graphene. *Journal of Applied Physics* **127** (2020). <https://doi.org/10.1063/1.5128329>
- 25 Friedman, J. R., Sarachik, M. P., Tejada, J., Maciejewski, J. & Ziolo, R. Steps in the hysteresis loops of a high-spin molecule. *Journal of Applied Physics* **79**, 6031-6033 (1996). <https://doi.org/10.1063/1.361837>
- 26 St Marie, L. *et al.* Nanostructured graphene for nanoscale electron paramagnetic resonance spectroscopy. *Journal of Physics-Materials* **3** (2020). <https://doi.org/10.1088/2515-7639/ab6af8>
- 27 El Fatimy, A. *et al.* Ultra-broadband photodetectors based on epitaxial graphene quantum dots. *Nanophotonics* **7**, 735-740 (2018). <https://doi.org/10.1515/nanoph-2017-0100>
- 28 El Fatimy, A. *et al.* Effect of defect-induced cooling on graphene hot-electron bolometers. *Carbon* **154**, 497-502 (2019). <https://doi.org/10.1016/j.carbon.2019.08.019>
- 29 Park, K., Pederson, M. R. & Hellberg, C. S. Properties of low-lying excited manifolds in Mn-12 acetate. *Physical Review B* **69** (2004). <https://doi.org/10.1103/PhysRevB.69.014416>
- 30 Petukhov, K., Hill, S., Chakov, N. E., Abboud, K. A. & Christou, G. Evidence for the S=9 excited state in Mn-12-bromoacetate measured by electron paramagnetic resonance. *Physical Review B* **70** (2004). <https://doi.org/10.1103/PhysRevB.70.054426>
- 31 Urdampilleta, M. *et al.* Molecular Quantum Spintronics: Supramolecular Spin Valves Based on Single-Molecule Magnets and Carbon Nanotubes. *INTERNATIONAL JOURNAL OF MOLECULAR SCIENCES* **12**, 6656-6667 (2011). <https://doi.org/10.3390/ijms12106656>
- 32 Switzer, E., Zhang, X., Turkowski, V. & Rahman, T. Mapping spin interactions from conductance peak splitting in Coulomb blockade. *PHYSICAL REVIEW B* **108** (2023). <https://doi.org/10.1103/PhysRevB.108.174438>
- 33 NOVAK, M., SESSOLI, R., CANESCHI, A. & GATTESCHI, D. MAGNETIC-PROPERTIES OF A MN CLUSTER ORGANIC-COMPOUND. *JOURNAL OF MAGNETISM AND MAGNETIC MATERIALS* **146**, 211-213 (1995).
- 34 Lecren, L. *et al.* Slow relaxation in a one-dimensional rational assembly of antiferromagnetically coupled [Mn₄] single-molecule magnets. *JOURNAL OF THE AMERICAN CHEMICAL SOCIETY* **127**, 17353-17363 (2005). <https://doi.org/10.1021/ja0551685>
- 35 Sessoli, R. *et al.* HIGH-SPIN MOLECULES - MN₁₂O₁₂(O₂CR)₁₆(H₂O)₄. *Journal of the American Chemical Society* **115**, 1804-1816 (1993). <https://doi.org/10.1021/ja00058a027>
- 36 Soler, M. *et al.* Single-molecule magnets:: Preparation and properties of mixed-carboxylate complexes Mn₁₂O₁₂(O₂CR)₈(O₂CR')₈(H₂O)₄. *Inorganic Chemistry* **40**, 4902-4912 (2001). <https://doi.org/10.1021/ic0104048>
- 37 Trammell, S. A. *et al.* Plasma-Modified, Epitaxial Fabricated Graphene on SiC for the Electrochemical Detection of TNT. *Sensors* **16** (2016). <https://doi.org/10.3390/s16081281>
- 38 Kresse, G. & Furthmuller, J. Efficiency of ab-initio total energy calculations for metals and semiconductors using a plane-wave basis set. *Computational Materials Science* **6**, 15-50 (1996). [https://doi.org/10.1016/0927-0256\(96\)00008-0](https://doi.org/10.1016/0927-0256(96)00008-0)

- 39 Kresse, G. & Furthmuller, J. Efficient iterative schemes for ab initio total-energy calculations using a plane-wave basis set. *Physical Review B* **54**, 11169-11186 (1996).
<https://doi.org/10.1103/PhysRevB.54.11169>
- 40 Blochl, P. E. PROJECTOR AUGMENTED-WAVE METHOD. *Physical Review B* **50**, 17953-17979 (1994). <https://doi.org/10.1103/PhysRevB.50.17953>
- 41 Kresse, G. & Joubert, D. From ultrasoft pseudopotentials to the projector augmented-wave method. *Physical Review B* **59**, 1758-1775 (1999). <https://doi.org/10.1103/PhysRevB.59.1758>
- 42 Klimes, J., Bowler, D. R. & Michaelides, A. Chemical accuracy for the van der Waals density functional. *Journal of Physics-Condensed Matter* **22** (2010). <https://doi.org/10.1088/0953-8984/22/2/022201>
- 43 Klimes, J., Bowler, D. R. & Michaelides, A. Van der Waals density functionals applied to solids. *Physical Review B* **83** (2011). <https://doi.org/10.1103/PhysRevB.83.195131>